# Kinetics of Proton Migration in Liquid Water

**Hanning Chen**[†] **and Gregory A. Voth**

*Center for Biophysical Modeling and Simulation and Department of Chemistry, University of Utah, Salt Lake City, Utah 84112-0850*

**Noam Agmon***

*The Fritz Haber Research Center and the Institute of Chemistry, The Hebrew University of Jerusalem, Jerusalem 91904, Israel*

*Received: August 23, 2009; Revised Manuscript Received: October 25, 2009*

We have utilized multistate empirical valence bond (MS-EVB3) simulations of protonated liquid water to calculate the relative mean-square displacement (MSD) and the history-independent time correlation function, $c(t)$, of the hydrated proton center of excess charge (CEC) with respect to the water molecule on which it has initially resided. The MSD is nonlinear for the first 15 ps, suggesting that the relative diffusion coefficient increases from a small value, $D_0$, at short separations to its larger bulk value, $D_\infty$, at large separations. With the ensuing distance-dependent diffusion coefficient, $D(r)$, the time dependence of both the MSD and $c(t)$ agrees quantitatively with the solution of a diffusion equation for reversible geminate recombination. This suggests that the relative motion of the CEC is not independent from the nearby water molecules, in agreement with theoretical and experimental observations that large water clusters participate in the mechanism of proton mobility.

Hydrogen bonds (HBs) in water are constantly breaking and forming.[1] The HB dynamics is in turn coupled to proton mobility in liquid water on a hierarchy of time scales.[2−5] The ongoing effort for understanding the microscopic mechanisms governing proton transport is motivated by its pivotal role in a myriad of processes, from acid−base reactions in solution to fuel cells and enzymatic catalysis.[6,7]

In order to elucidate the HB kinetics from a molecular dynamics (MD) simulation of bulk liquid water,[8] the "history independent" pair correlation function, $c(t)$, was extensively utilized.[9−16] This function depicts the probability for a specific ("tagged") water−molecule pair that was bound at time $t = 0$ to be bound at some later time, $t$. The time course of $c(t)$ was found to be highly nonexponential.[9] Luzar and Chandler[10] suggested that this is due to the (translational) diffusion of water molecules, although there was previously no consensus concerning the precise functional dependence of its time course.[10,12]

Recently, it was demonstrated[17] that $c(t)$ conforms quantitatively to a diffusion-theoretical expression for the binding probability of a reversible geminate pair,[18−21] a model previously introduced in refs 22−24. The decay of $c(t)$ starts off as an exponential (or, perhaps, as a stretched exponential[12]) but rapidly approaches an asymptotic $t^{-3/2}$ behavior that depicts the probability of a random walker in three dimensions to return to the origin of its random walk.[25] The random walk here occurs in the relative separation coordinate, $r$, of the two tagged water molecules. Once they return to a distance smaller than a cutoff distance, $R$, the original HB can reform. Therefore $c(t)$ is determined by the relative diffusion constant, $D$, and by the two rate coefficients, $k_d$ and $k_a$, for HB dissociation and association, respectively.

A correlation function approach was recently applied to analyze the dynamical features of proton and hydroxide mobility in liquid water by Chandra et al.[26] These authors generalized this approach from simple hydrogen-bond kinetics to proton migration kinetics by introducing appropriate population functions for topological defects. Both the (faster) history-dependent and (slower) history-independent $c(t)$ were discussed there and suggested to conform to a biexponential time course. However, results for the latter were not shown, perhaps because of the relatively short trajectories available from the computationally demanding ab initio molecular dynamics (AIMD) procedure.[27] Here, we report results for the history-independent $c(t)$ to asymptotically long times (500 ps), utilizing the computationally more efficient multistate empirical valence bond model (MS-EVB).[3,28,29] Given the results for pure water,[17] our goal is to check whether the proton−water $c(t)$ also conforms to the diffusion model of reversible geminate recombination, with its asymptotic $t^{-3/2}$ behavior.

The experience from applying the reversible diffusion model to excited-state proton transfer to solvent[23,24,30] has taught us the importance of basing the kinetic analysis on an independent determination of the relative diffusion coefficient. We have therefore also calculated, from the same trajectory data, the relative mean-square displacement (MSD) of the hydrated proton center of excess charge (CEC) and the water oxygen to which it was originally attached. To our knowledge, this relative MSD has not been reported before. We show below that it is nonlinear, suggesting a distance dependence in the relative diffusion coefficient, from small values at short separations to its bulk value, $D_\infty$, at larger separations. This distance dependence is in accord with estimates[31] and calculations[32] indicating substantial HB strengthening near the hydrated proton. Because of this effect, the motions of the delocalized proton and the water

* To whom correspondence should be addressed. E-mail: agmon@fh.huji.ac.il.

[†] Present address: Department of Chemistry, Northwestern University, Evanston, IL 60208-3113.

10.1021/jp908126a 
Published on Web 12/04/2009

molecule are not independent at small separations. This, we argue, is in line with recent computational[4] and experimental[33] assessments that large water molecule clusters are involved in the mechanism underlying proton mobility.

### Simulation Protocol

The simulations were performed as follows. A cubic simulation box with a 18.621 Å long edge consists of 216 SPC/Fw[15] water molecules and an excess proton. A total of 10 independent trajectories with uncorrelated initial configurations were generated for each one of the following temperatures: 280, 300, and 320 K. The MS-EVB3 model[29] was used to describe the proton dynamics, and the DLEVB package[34] was employed to perform all of the calculations. For each trajectory, a 5 ns production run in the microcanonical (NVE) ensemble was carried out after a 0.5 ns equilibration run in the canonical (NVT) ensemble, where a Nosé−Hoover thermostat[35] with a relaxation time of 0.2 ps was utilized to maintain the system's temperature. The MD integration time step was 0.5 fs, and a three-dimensional periodic boundary condition was applied. The long-range electrostatics were treated by the Ewald summation,[36] and a spherical cutoff scheme with a radius of 9.0 Å was used for the van der Waals interactions. During the production runs, the atomic coordinates were saved every 10 time steps, making a total of 1 000 000 configurations available for postcalculation analysis for each trajectory. The multiple-time-origin method was applied for enhanced statistical sampling, which amounts to about 100 000 trajectory segments of 500 ps at each temperature. For further treatment, the coordinates within the periodic box were transformed to the "real" particle coordinates in infinite non-periodic space.[17,36]

To check for the possible influence of the simulation box size on the results,[37] we have also propagated five 5 ns trajectories at 300 K for 290 water molecules and an excess proton in a cubic box of edge length 20.46 Å. The results generally agree with those of the smaller box within statistical noise, so we concluded that the differences in box size are too small for observing box size effects. Calculations with even larger box sizes were unrealistic in terms of computer time.

In the MS-EVB method, the system is represented at any time $t$ by a linear combination of $N$ states, each corresponding to one hydrogen-bonding arrangement, with one of the oxygens assigned the role of the hydronium. If $c_i$ denote the coefficients of this expansion ($\sum_{i=1}^{N} c_i^2 = 1$, $i = 1,\cdots, N$), then the "pivot oxygen" (PO) is defined as that of the maximal $c_i^2$. Denote by $\mathbf{r}_i$ the position vector for the center of charge of the hydronium of the $i$th EVB state at any time $t$. Then, we define the center of excess charge (CEC), $\mathbf{r}_{CEC}$, as the weighted average of the center of charge in all of the EVB states:

$$\mathbf{r}_{CEC} \equiv \sum_{i=1}^{N} c_i^2 \mathbf{r}_i \tag{1}$$

This is fairly close to the coordinate vector of the PO but is modulated by the (typically asymmetric) delocalization of the positive charge defect over many EVB states. Thus, the CEC is a representation of the most probable position of the excess proton.

For a continuous simulation trajectory segment that starts at a time arbitrarily denoted by $t = 0$ and ends at 500 ps, the PO at $t = 0$ is denoted by O*. Its position vector at any later time $t$ is $\mathbf{r}_{O^*}(t)$. The separation between the CEC and O* at any time is thus:

$$r(t) \equiv |\mathbf{r}_{CEC}(t) - \mathbf{r}_{O^*}(t)| \tag{2}$$

We note that $r(0) > 0$, because the environment of the hydronium is nonsymmetric and there is always one water ligand that is closer than the other two.[38] The CEC is displaced in its direction.

From the trajectory data, two functions related to the separation $r(t)$ were calculated:

(a) The relative "mean square displacement" (MSD), $\langle r(t)^2 \rangle$, where the averaging $\langle ... \rangle$ is performed over all trajectory frames at time $t$. The diffusion coefficient, $D$, is then calculated from its slope at any value of $t$, concomitant with the Einstein relation

$$D(t) = \frac{1}{6}\frac{d\langle r(t)^2 \rangle}{dt} \tag{3}$$

(b) The history-independent time correlation function $c(t)$ is defined as $\langle \delta(t) \rangle$, where $\delta(t) = 1$ if $r(t) < r_{cut}$ and zero otherwise.

According to the radial distribution function (RDF) calculation, the cutoff radius $r_{cut}$ was chosen to be 1.60 Å, the first minimum of the RDF between the CEC and its neighboring oxygen atoms, to reflect the approximate radius of the first water solvation shell of the excess proton.

In addition, we have calculated separately the Debye relaxation time, $\tau_D$, for the underlying SPC/Fw flexible simple point-charge water model.[15] It is obtained by exponentially fitting the normalized dipole autocorrelation function, $\varphi(t)$, which is defined as

$$\varphi(t) \equiv \frac{\langle M(t)M(0) \rangle - \langle M(0) \rangle^2}{\langle M(0)^2 \rangle - \langle M(0) \rangle^2} \tag{4}$$

where $M(t)$ is the total dipole moment of the water molecules in the simulation box at time $t$ for a 20 ns long trajectory. The subtraction of $\langle M(0) \rangle^2$ is because the average dipole moment does not precisely vanish in a finite simulation box.

### Diffusion Theory

In the theoretical treatment of $c(t)$, we envision a geminate reversible reaction:[22,23]

$$C \underset{k_a}{\overset{k_d}{\rightleftarrows}} A + B \tag{5}$$

where A is a specific water molecule, B the excess charge, and C the hydronium species formed when this charge is located on the specified water molecule. Thus, $k_d$ and $k_a$ are dissociation and association rate constants, respectively. The history-independent correlation function, $c(t)$, depicts the probability of observing state C, in which the pair at time $t$ is bound irrespective of its history (which could have involved numerous dissociation−association events).

A and B are assumed[18−21] to obey a diffusion equation in their relative separation, $r \geq R$, with $p(r, t)$ denoting the probability of the pair assuming a separation $r$ at time $t$:

$$\partial p(r,t)/\partial t = \mathscr{L} p(r,t) - W_a(r)p(r,t) + W_d(r)c(t) \tag{6a}$$

$$dc(t)/dt = 4\pi \int_R^\infty r^2 dr W_a(r) p(r,t) - k_d c(t) \tag{6b}$$

In the absence of long-range interactions between A and B, the operator $L$ is the three-dimensional Laplacian,

$$\mathscr{L} = r^{-2}\frac{\partial}{\partial r} D(r) r^2 \frac{\partial}{\partial r} \tag{7}$$

The pair kinetics is dictated by their relative translational diffusion coefficient, $D(r)$, which may (or may not) depend on

$r$. When the motion of A and B is uncorrelated, with diffusion constants $D_A$ and $D_B$, respectively, one can show that their sum

$$D_\infty \equiv D_A + D_B \tag{8}$$

is equal to the relative diffusion coefficient (see Ch. 9 in ref 39). A distance dependence in $D(r)$ may arise if the motion of the two particles at short distances is not independent. In such a case, one may still expect $D_\infty$ to depict the relative diffusion coefficient at large separations (hence at long times).

The reversible reaction within the pair[22] is depicted in eq 6a by the "sink functions", $W_d(r)$ and $W_a(r)$, for dissociation and association, respectively. The coupled ordinary differential eq 6b describes the temporal evolution of their binding probability, $c(t)$. When the reaction is restricted to occur at the contact distance, $R$, these sink functions become

$$W_d(r) = k_d \frac{\delta(r-R)}{4\pi R^2}, \quad W_a(r) = k_a \frac{\delta(r-R)}{4\pi R^2} \tag{9}$$

where $\delta(x)$ is the Dirac delta-function. Because the reaction is depicted already by the sink terms, a reflecting boundary condition is imposed at $r = R$, namely $\partial p(r,t)/\partial r|_{r=R} = 0$ (alternately, the reaction can be introduced as a back-reaction boundary condition[22]). Initially, $p(r,0) = 0$ and $c(0) = 1$, because we start here from a bound pair.

When $D(r)$ is constant, this set of equations can be solved analytically.[18−21] When $D(r)$ varies with distance, an analytic solution usually does not exist. The full solution in this case can be obtained numerically with the freely available Windows application for solving the spherically symmetric diffusion equation (SSDP, ver. 2.66).[40] Yet, the asymptotic long-time solution may still be obtained analytically. Starting with the asymptotic solution for a fixed diffusion constant,[19,24] we introduce into it the limiting value $D_\infty$, where $D(r) \to D_\infty$ as $r \to \infty$, so that

$$c(t) \sim K_{eq}(4\pi D_\infty t)^{-3/2} \tag{10}$$

Here, $K_{eq} \equiv k_a/k_d$ is the equilibrium constant for the reversible reaction in the association direction.

The relative MSD for the pair can be calculated from its density distribution, $p(r,t)$, according to its definition

$$\langle r^2(t)\rangle \equiv \int_R^\infty r^2 p(r,t) 4\pi r^2 dr \tag{11}$$

This calculation can also be done within SSDP. In this way, both attributes, the correlation function and MSD, which were calculated from the same set of trajectories, are modeled by the *same* set of coupled differential equations, eqs 6a and 6b.

## Results

In this section, we present the simulation results for both $\langle r^2(t)\rangle$ and $c(t)$ at different temperatures, $T$, and analyze them by the above diffusion model for reversible geminate recombination. The novel aspect of our presentation, as compared with previous work,[18−24] is the introduction of a distance-dependent diffusion coefficient, $D(r)$, as a means of explaining simultaneously both types of data. To further reduce the number of adjustable parameters, the contact distance, $R$ in eq 9, is assumed to be identical to the $r_{cut}$ value used in the simulations; hence $R = 1.6$ Å. Modifying it can be compensated by a concomitant change in $k_a$, without an observable effect on the quality of fit.

**Mean Square Displacements.** The MSD of either the CEC or the CEC−PO pair is not a simple linear function of time. Such behavior prevails only at long times. At short times, we see two additional phenomena. In the subpicosecond time regime

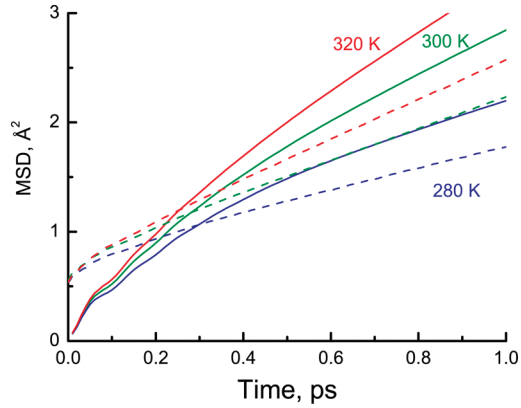


**Figure 1.** Short-time behavior of the mean square displacement (MSD) for the excess proton CEC (full lines) and relative CEC−PO distance (dashed lines), from classical MS-EVB3 simulations of protonated liquid water at 280 (blue), 300 (green), and 320 K (red). A simulation box of linear dimension 18.621 Å was utilized.

(Figure 1), the MSD is determined from the dynamics of the "special pair dance",[5] in which one of the three water ligands of the Eigen cation, $H_9O_4^+$, is closer than the other two, forming a "special pair".[38] As a result, the CEC is displaced from the PO toward the hydrogen atom forming the HB with the closest water ligand. This is manifested in the CEC−PO MSD (dashed lines), which starts at $t = 0$ from a nonzero value of 0.54 Å$^2$, corresponding to an initial average separation between the CEC and the PO, $r(0) = 0.734$ Å. In contrast, the absolute CEC MSD starts from zero (because the reference is its own initial location), but due to the "special pair dance", which interchanges the special partners on a 50 fs time scale (per exchange),[5] the CEC essentially hops between positions close to the three hydrogens of the hydronium. This results in a fast initial dynamic increase in the CEC MSD.

At somewhat longer times, the absolute CEC MSD becomes a linear function of time, but the relative one does not. Figure 2 shows the time dependence of the relative MSD of the CEC−PO pair, as compared with the absolute MSDs for the CEC and for bulk water, in the picosecond time regime. The relative MSD starts off with a small slope, approaching at long times a linear dependence that is roughly the (shifted) sum of the two absolute MSDs (dashed line). This means that the diffusion constant varies with time, from a small value, $D_0$, at short times, to a larger value, $D_\infty$, at long times when eq 8 is approximately obeyed.

We interpret the time variation in $D(t)$ as arising from a distance-dependent $D(r)$, which is due to the fact that diffusion is impeded at short separations, due to the stronger HBs in the hydronium inner solvation shells.[32] We have constructed a model $D(r)$ as follows. First, we have fitted the relative MSD to the three parameter equation

$$\langle [r(t) - r(0)]^2\rangle/6 = D_\infty t + \tau(D_\infty - D_0)(e^{-t/\tau} - 1) \tag{12}$$

By differentiating, as in eq 3, it can be seen that $D(t) = D_\infty - (D_\infty - D_0)e^{-t/\tau}$, so that $D_0$ and $D_\infty$ are its limiting values when $t \to 0$ and $t \to \infty$, respectively, whereas $\tau$ is the time constant for switching between the two limits. The fit for the 300 K data is shown by the dotted black line in Figure 2. It applies a value of $D_\infty$ obtained by fitting the whole data set, up to 500 ps.

Next, we transform $D(t)$ into a $D(r)$: because the nonlinearity in the MSD is a short-time effect, we use its short-time limit,

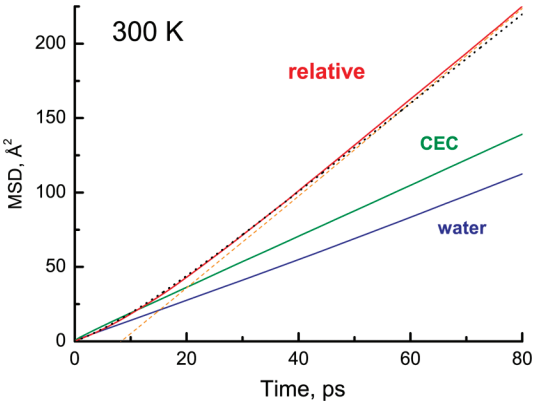


**Figure 2.** Mean square displacement (MSD) for relative CEC−PO diffusion as a function of time (red line), from classical MS-EVB3 simulations of protonated liquid water at 300 K in a box of linear dimension 18.621 Å. The nonzero $t = 0$ value, 0.54 Å$^2$, has been subtracted (a minute correction, hardly visible on the present scale). Absolute MSDs (relative to a fixed origin in space) are shown for the center of excess charge (CEC, green) and bulk water (blue, from a simulation on a system consisting of 216 SPC/Fw water molecules[15] without an excess proton). Red dashed line is the sum of the two absolute MSDs, minus a constant of 28 Å$^2$. Dotted black line is a fit to eq 12 (up to 500 ps) with $D_0$, $D_\infty$ from Table 1, $\tau = 13$ ps and $r(0) = 0.734$ Å (the initial average CEC−PO separation in our simulations).

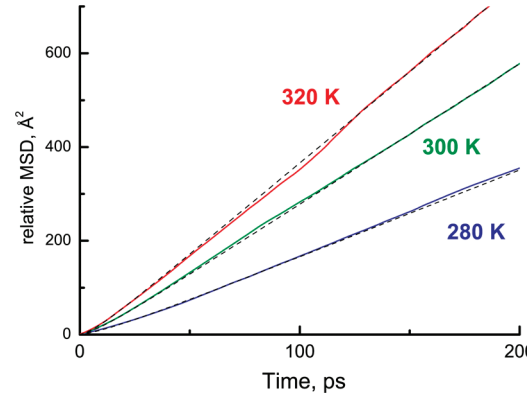


**Figure 3.** Mean square displacement (MSD) for relative CEC−PO diffusion as a function of time, from classical MS-EVB3 simulations at three temperatures (color-coded lines). Dotted black lines are a fit to the solution of the geminate recombination model, eq 6 with $D(r)$ from eq 13 and relevant parameters in Table 1.

$\langle r(t)^2\rangle \approx 6D_0t$, to eliminate $t$. In a mean-field sense, we equate the average with the momentary value to obtain

$$D(r) = D_\infty - (D_\infty - D_0)\exp[-[r - r(0)]^2/(6D_0\tau)] \quad (13)$$

Next, we introduce $D(r)$ into the diffusion operator, eq 7. Maintaining the values of $D_0$ and $D_\infty$ obtained by fitting eq 12 to the relative MSD, we then calculate $\langle r^2(t)\rangle$ via eq 11 from the time-dependent solution, $p(r, t)$, of the diffusion model in eq 6a. Because the dissociation process (rate constant $k_d$) slows down the spread in $p(r, t)$, we need to readjust $\tau$ to a smaller value than that obtained by fitting the empirical eq 12 to $\langle r^2(t)\rangle$.

Figure 3 shows the relative MSDs at all three temperatures, as obtained from our MS-EVB3 simulations (color lines) on the picosecond time scale. The dashed black lines show $\langle r^2(t)\rangle$, as calculated by the SSDP software[40] for the reversible geminate recombination model in eqs 6a and 6b. The rate parameters in this model, $k_d$ and $k_a$, were chosen so that the *same* solution reproduces also $c(t)$ below. From the figure, it can be seen that this model with the distance dependent $D(r)$ reproduces the simulation data to within statistical error.

The absolute diffusion coefficients and the parameters for the relative diffusion coefficient in eq 13 are collected in Table 1. The table shows that although eq 8 is approximately obeyed, a closer inspection reveals that $D_\infty < D_{CEC} + D_{water}$ by a small amount (0.03 Å$^2$/ps) at all three temperatures. We attribute this to finite size effects of the simulation box,[37] which induces some correlations between the CEC and PO. For this reason, we have performed the simulation within the larger box (of 20.46 Å), but the size difference is not sufficient to demonstrate the convergence in $D_\infty$ (in fact, results for the two boxes were identical within statistical noise). Simulations with a much larger box are presently not practical, so we defer the detailed study of the system-size effect to future work.

Figure 4 shows the temperature dependence of $D_\infty$ and $D_{CEC}$ in the range 280−320 K. As a first approximation, we fit them to an Arrhenius equation with an activation energy of 11.8 kJ/mol. However, both diffusion constants deviate somewhat from a linear Arrhenius plot. The activation energy for the water diffusion constants in Table 1 is higher, approximately 15 kJ/mol.

The relaxation time, $\tau$, for the relative diffusion constant is shorter than the Debye relaxation time, $\tau_D$, calculated for the underlying SPC/Fw water model,[15] yet fortuitously close to the experimental $\tau_D$ values (see Table 1).[41,42] However, at 280 K, $\tau_D$ slows down more conspicuously than $\tau$, and $\varphi(t)$ from eq 4 deviates from exponential. A similar effect was previously noted in comparing experimental $\tau_D$ with proton hopping times (see Figure 1 in ref 43). Figure 5 shows the temperature dependence of the two relaxation times. While $\tau_D$ is not of an Arrhenius form, $\tau$ is. Its activation energy is 12.9 kJ/mol, close to that obtained for $D_\infty$.

**Correlation Function.** Figure 6 shows the CEC−PO correlation function at room temperature, on a log−log plot covering 500 ps in time and 4 orders of magnitude in $c(t)$ decay. Just like the history-independent correlation function

**TABLE 1: Absolute CEC and Bulk Water Diffusion Constants (in Units of Å$^2$/ps) and Parameters for the Relative Diffusion Coefficient (eq 12), as Determined from the Simulation Data (Figure 3)[a]**

| $T$ (K) | $D_{CEC}$ | $D_{water}$ | sum | $D_0$ | $D_\infty$ | $\tau$ (ps) | $\tau_D$[b] (ps) | $\tau_D$[c] (ps) |
|---|---|---|---|---|---|---|---|---|
| 280 | 0.195 | 0.15 | 0.34 | 0.14 | 0.31 | 12 | 21 | 14 |
| 300 | 0.285[d] | 0.24[d] | 0.53 | 0.24 | 0.50 | 8 | 12[e] | 8 |
| 320 | 0.34 | 0.33 | 0.67 | 0.25 | 0.65 | 6 | 7.3 | 6 |

[a] Error bars on the diffusion constants are about ±0.01. Also given are the Debye relaxation times for water at the relevant temperatures (theoretical and experimental). [b] Calculated for the SPC/Fw water model.[15] [c] Experimental, interpolated from refs 41 and 42. [d] Values essentially identical to those reported in ref 29 for a MS-EVB3 simulation involving 216 water molecules plus a proton. [e] As compared with 9.5 ps calculated in ref 15.

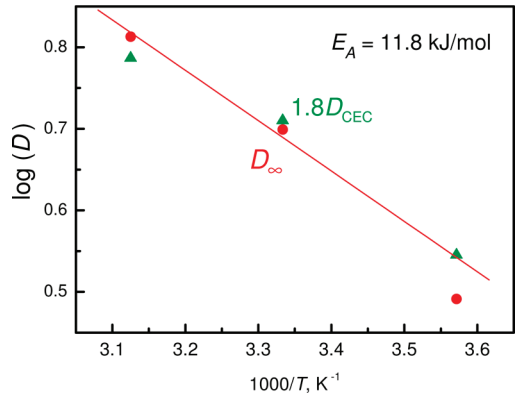


**Figure 4.** Temperature dependence of the diffusion coefficients (Table 1, in units of cm$^2$/s). Shown are the long-time limit of the relative diffusion coefficient ($D_\infty$, red circles) and the CEC diffusion coefficient multiplied by 1.8 (green triangles). The linear fit (red line) gives an activation energy of 11.8 kJ/mol.

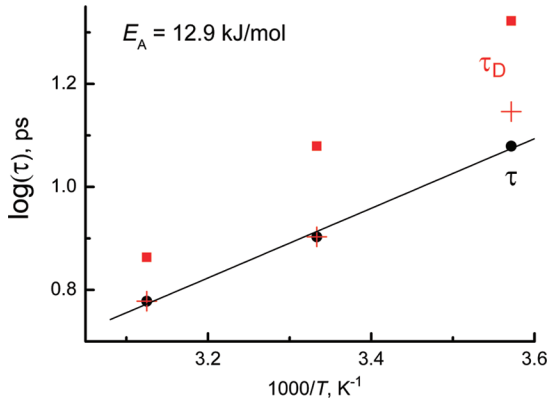


**Figure 5.** Temperature dependence of the relaxation time for $\tau$ of eq 13 (circles), compared with the Debye relaxation time, $\tau_D$ (red squares, simulation; red crosses, experiment), for the underlying water model (data from Table 1). The linear fit (line) gives an activation energy of 12.9 kJ/mol for $\tau$.

for water−water pairs,[17,44] $c(t)$ here is highly nonexponential. A biexponential function previously advocated,[26]

$$c(t) \approx a_1\exp(-t/t_1) + a_2\exp(-t/t_2) \qquad (14)$$

where $(a_1 + a_2 = 1)$ describes only the first decade of the decay (magenta dashed line). It should be realized that the AIMD calculations utilized in ref 26 are computationally expensive and thus cannot reveal the long-time power-law tail (which is clearly evident as an asymptotically straight line on the log−log scale). The MS-EVB simulations are significantly faster, and even then, months of continuous computation were required to generate the complete time-dependence revealed in this figure.

In contrast to the biexponential function, the reversible diffusion model with the distance-dependent diffusivity in eq 13 describes the whole time dependence (full black line). The dashed red lines show the solution to the diffusion model with the same parameters, but with a distance-independent diffusion constant, equal either to the short-distance ($D_0$) or long-distance ($D_\infty$) limits of $D(r)$. As expected, the solution with $D = D_0$ provides a short-time approximation to the full solution, whereas that with $D = D_\infty$ provides a long-time approximation, particularly in the asymptotic regime where it approaches the asymptotic behavior of eq 10. The full solution using $D(r)$, which interpolates between these two values, naturally interpolates between the two limiting solutions. In the switch-over

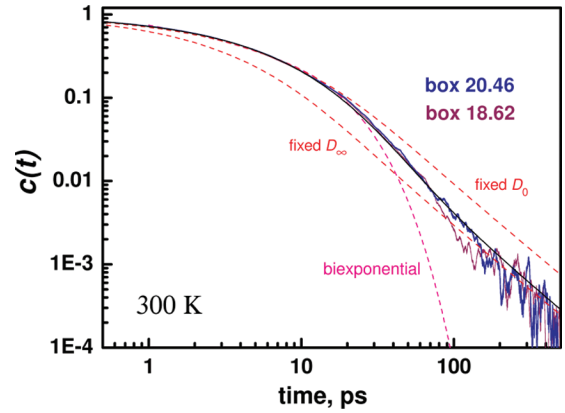


**Figure 6.** CEC−PO history-independent correlation function from classical MS-EVB3 simulations (blue and purple lines), depicted on a log−log scale. A dashed magenta line shows the best fit to a biexponential function (restricted to pass through $c(0) = 1$) in the range 0−60 ps. The parameters in eq 14 are $a_1 = 0.464$, $a_2 = 0.534$, $t_1 = 1.65$ ps, and $t_2 = 11.1$ ps. Full black line is a fit to the diffusion model, eqs 6, 7, and 9, with $D(r)$ from eq 13 and parameters from Table 1. The dashed red lines are the solutions of the same equations with a fixed diffusion constant equal to either $D_0$ or $D_\infty$. In all cases, the "contact distance" $R = 1.6$ Å, and the dissociation and association rate parameters are $k_d = 1.07$ ps$^{-1}$ and $k_a/(4\pi R^2) = 1.6$ Å/ps, respectively.

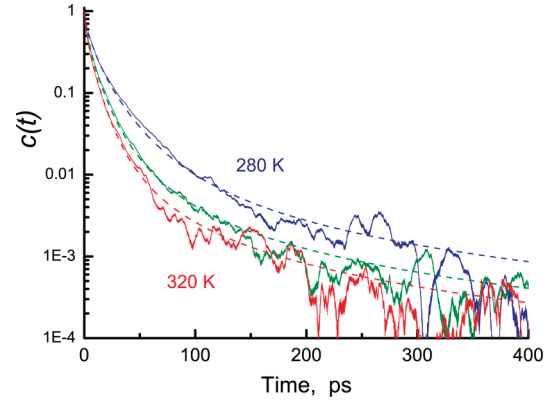


**Figure 7.** CEC−PO pair correlation functions from classical MS-EVB3 simulations at three temperatures (colored lines) on a semilog scale. Fits to the diffusion model (dashed lines) are as described in Figure 6 and with the same values of $R$, $k_d$, and $k_a$.

region, $c(t)$ therefore decays faster than expected from a diffusion model with a fixed diffusion constant.

Figure 7 shows our fits at all three temperatures on a semilogarithmic scale. The parameters for $D(r)$ were taken from Table 1, whereas $k_d$ and $k_a$ were kept fixed for all $T$. Nevertheless, these rate parameters are not necessarily temperature independent. Rather, the fit is insensitive to their precise values as long as their ratio, $K_{eq} \equiv k_a/k_d$, is maintained constant. Thus, from the fit, we can only conclude that $K_{eq}$ here is nearly temperature independent, so that the slightly different asymptotic limits approached by the data in Figure 7 are due predominantly to the temperature dependence of $D_\infty$ in eq 10. From the best-fit rate constants, the value of $K_{eq}[H_2O] = (k_a/k_d)N/V = 1.29$, which is close to unity. This fact, and particularly its temperature independence, can be rationalized by noting that both association and dissociation directions are governed by the *same* process of proton hopping between two neighboring water molecules. Thus, in essence, there is only *one* rate parameter involved in the $c(t)$ dynamics.

## Discussion and Conclusion

The history-independent correlation function of two tagged particles in solution is dictated by translational diffusion, as suggested,[10] and demonstrated quantitatively[17] for water molecule pairs in liquid water. Here, we showed that $c(t)$ for the hydronium (CEC) and "pivot oxygen" (PO, the atom on which the hydronium initially resides) pair obeys similar kinetics. By using extensive MS-EVB3 simulations, $c(t)$ was calculated to long times (500 ps) where the expected asymptotic $t^{-3/2}$ behavior for reversible diffusion influenced reactions comes into play.

At intermediate times, $c(t)$ decays too fast in comparison with a simple diffusion model involving a fixed diffusion constant (and no potential of interaction), see Figure 6. We have found that this behavior has the same physical origin as the nonlinearity in the relative MSD that we observed in the picosecond time regime. Both are consistently explained by a distance-dependent diffusion coefficient, $D(r)$, for the relative CEC−PO motion depicted in eq 13. With increasing pair separation, $r$, it switches (exponentially in $r^2$) from a small value near contact, $D_0$, to a larger value, $D_\infty$, at large separations.

The origin of the variation in $D(r)$ can be traced to the enhanced hydrogen bonding near the hydronium.[31] By using MS-EVB2 simulations, the HB strength in the first hydronium solvation shell was found[32] to be more than double that of bulk water. Thus, when the hydronium "sits" on the PO, the latter is essentially immobilized. Consequently, the main contribution to $D(r)$ at small separations comes from CEC diffusion, so that $D_0 \approx D_{CEC}$. At large separations, the CEC and PO move independently, so that $D_\infty \approx D_{CEC} + D_{water}$ (with small deviations tentatively attributed to finite-size effects).

How far need the CEC and PO separate for uncorrelated diffusion to occur? From Figure 2, it is seen that, at 300 K, when $t = \tau = 8$ ps, $\langle r^2 \rangle = 14$ Å$^2$, which corresponds to a separation of 3.7 Å. From Table 1, we find similarly that $(6D_{CEC}\tau)^{1/2} = 3.7$ Å at this temperature (this value changes only slightly with $T$). The hopping distance for the proton within the Zundel-like transferring complex is 2.5 Å.[31] Hence, by time $\tau$, the CEC has executed more than one jump. Yet, at that time, the relative MSD is still far from its limiting behavior (see Figure 2). Therefore, the CEC must execute at least two jumps, leaving the PO in its second solvation shell, before bulklike behavior sets in.

Experimentally, HBs in the inner solvation shell of cations are stronger, as deduced from the slower water rotation there.[45] For most cations, the effect does not extend beyond the first-shell ligands,[45] yet for the more delocalized protonic charge it could. Alternately, even if the HB strength in the second shell is not significantly larger than in the bulk, the motion of these water molecules is still correlated with that of the excess proton. This agrees with the observation of Lapid et al.,[4] from "bond-order analysis" of MS-EVB2 simulations, that concerted motion in the first two solvation shells of the reactive intermediate, the protonated water-dimer complex ("Zundel cation"), accompanies successful proton hopping events. Water clusters containing some 20 water molecules may be involved in this inner core dynamics.

Interestingly, recent terahertz time-domain dielectric relaxation experiments in acidified water[33] find depolarizations attributed to about 4 water molecules that are immobilized near the hydronium and 15 more that participate kinetically in proton mobility. This corroborates the above theoretical observations and lends support to the model of distance-dependent mutual diffusivity.

The relative diffusion coefficient enters into the analysis of experiments of excited-state proton transfer (ESPT) to solvent,[30] yet a distant-dependent $D(r)$ has not been invoked there. Observing such an effect may require monitoring the ESPT reaction on the ultrafast time scale of say 100 fs to 10 ps. Indeed, when methods (such as pump−probe) with faster temporal resolution are applied, some photoacids show additional fast components in their kinetics. These have been attributed to either solvation[46] or, more recently, a short-lived contact-ion pair between the hydronium and the excited anion.[47] Such a contact ion-pair, if it exists, may be a manifestation of the slower hydronium diffusion while it is in the solvation shell of the anion.

**Acknowledgment.** We thank Omer Markovitch for discussions at an early stage of this project. This research was supported by the United States-Israel Binational Science Foundation (BSF) Grant 2006067 (N.A. and G.A.V.) and the United States National Science Foundation Grant CHE-0719522 (G.A.V.) The Fritz Haber Center is supported by the Minerva Gesellschaft für die Forschung, München, FRG.

## References and Notes

(1) Rahman, A.; Stillinger, F. H. *J. Am. Chem. Soc.* **1973**, *95*, 7943.
(2) Agmon, N. *Chem. Phys. Lett.* **1995**, *244*, 456.
(3) Day, T. J. F.; Soudackov, A. V.; Čuma, M.; Schmitt, U. W.; Voth, G. A. *J. Chem. Phys.* **2002**, *117*, 5839.
(4) Lapid, H.; Agmon, N.; Petersen, M. K.; Voth, G. A. *J. Chem. Phys.* **2005**, *122*, 014506.
(5) Markovitch, O.; Chen, H.; Izvekov, S.; Paesani, F.; Voth, G. A.; Agmon, N. *J. Phys. Chem. B* **2008**, *112*, 9456.
(6) Swanson, J. M. J.; Maupin, C. M.; Chen, H.; Petersen, M. K.; Xu, J.; Wu, Y.; Voth, G. A. *J. Phys. Chem. B* **2007**, *111*, 4300.
(7) Marx, D. *ChemPhysChem* **2006**, *7*, 1848 Addendum. ibid. *8*, 209.
(8) Stillinger, F. H. *Adv. Chem. Phys.* **1975**, *31*, 1.
(9) Rapaport, D. C. *Mol. Phys.* **1983**, *50*, 1151.
(10) Luzar, A.; Chandler, D. *Nature* **1996**, *379*, 55.
(11) Luzar, A. *J. Chem. Phys.* **2000**, *113*, 10663.
(12) Starr, F. W.; Nielsen, J. K.; Stanley, H. E. *Phys. Rev. E* **2000**, *62*, 579.
(13) Xu, H.; Stern, H. A.; Berne, B. J. *J. Phys. Chem. B* **2002**, *106*, 2054.
(14) Raiteri, P.; Laio, A.; Parrinello, M. *Phys. Rev. Lett.* **2004**, *93*, 087801.
(15) Wu, Y.; Tepper, H. L.; Voth, G. A. *J. Chem. Phys.* **2006**, *124*, 024503.
(16) Lee, H.-S.; Tuckerman, M. E. *J. Chem. Phys.* **2007**, *126*, 164501.
(17) Markovitch, O.; Agmon, N. *J. Chem. Phys.* **2008**, *129*, 084505.
(18) Agmon, N.; Weiss, G. H. *J. Chem. Phys.* **1989**, *91*, 6937.
(19) Agmon, N.; Szabo, A. *J. Chem. Phys.* **1990**, *92*, 5270.
(20) Kim, H.; Shin, K. J. *Phys. Rev. Lett.* **1999**, *82*, 1578.
(21) Gopich, I. V.; Agmon, N. *J. Chem. Phys.* **1999**, *110*, 10433.
(22) Agmon, N. *J. Chem. Phys.* **1984**, *81*, 2811.
(23) Pines, E.; Huppert, D.; Agmon, N. *J. Chem. Phys.* **1988**, *88*, 5620.
(24) Agmon, N.; Pines, E.; Huppert, D. *J. Chem. Phys.* **1988**, *88*, 5631.
(25) Weiss, G. H. *Aspects and Applications of the Random Walk*; North-Holland: Amsterdam, 1994.
(26) Chandra, A.; Tuckerman, M. E.; Marx, D. *Phys. Rev. Lett.* **2007**, *99*, 145901.
(27) Car, R.; Parrinello, M. *Phys. Rev. Lett.* **1985**, *55*, 2471.
(28) Schmitt, U. W.; Voth, G. A. *J. Chem. Phys.* **1999**, *111*, 9361.
(29) Wu, Y.; Chen, H.; Wang, F.; Paesani, F.; Voth, G. A. *J. Phys. Chem. B* **2008**, *112*, 467.
(30) Agmon, N. *J. Phys. Chem. A* **2005**, *109*, 13.
(31) Agmon, N. *J. Chim. Phys. Phys.-Chim. Biol.* **1996**, *93*, 1714.
(32) Markovitch, O.; Agmon, N. *J. Phys. Chem. A* **2007**, *111*, 2253.
(33) Tielrooij, K. J.; Timmer, R. L. A.; Bakker, H. J.; Bonn, M. *Phys. Rev. Lett.* **2009**, *102*, 198303.
(34) Smondyrev, A. M.; Voth, G. A. *Biophys. J.* **2002**, *82*, 1460.
(35) Nosé, S. *Mol. Phys.* **1984**, *52*, 255.
(36) Rapaport, D. C. *The Art of Molecular Dynamics Simulations*, 2nd ed.; Cambridge University Press: Cambridge, U.K., 2004.
(37) Yeh, I.-C.; Hummer, G. *J. Phys. Chem. B* **2004**, *108*, 15873.

(38) Tuckerman, M.; Laasonen, K.; Sprik, M.; Parrinello, M. *J. Phys. Chem.* **1995**, *99*, 5749.
(39) Rice, S. A. Diffusion-Limited Reactions. In *Comprehensive Chemical Kinetics*; Elsevier: Amsterdam, 1985; Vol. 25.
(40) Krissinel', E. B.; Agmon, N. *J. Comput. Chem.* **1996**, *17*, 1085.
(41) Buchner, R.; Barthel, J.; Stauber, J. *Chem. Phys. Lett.* **1999**, *306*, 57.
(42) Beneduci, A. *J. Mol. Liq.* **2008**, *138*, 55.
(43) Agmon, N. *J. Phys. Chem.* **1996**, *100*, 1072.
(44) Han, S.; Kumar, P.; Stanley, H. E. *Phys. Rev. E* **2009**, *79*, 041202.
(45) Omta, A. W.; Kropman, M. F.; Woutersen, S.; Bakker, H. J. *Science* **2003**, *301*, 347.
(46) Tran-Thi, T.-H.; Gustavsson, T.; Prayer, C.; Pommeret, S.; Hynes, J. T. *Chem. Phys. Lett.* **2000**, *329*, 421.
(47) Leiderman, P.; Genosar, L.; Huppert, D. *J. Phys. Chem. A* **2005**, *109*, 5965.

JP908126A